jove

# High-Resolution Studies of Proteins in Natural Membranes by Solid-State NMR

**David Beriashvili**[1], **Raymond D. Schellevis**[1], **Federico Napoli**[1], **Markus Weingarth**[1], **Marc Baldus**[1]

[1] NMR Spectroscopy, Bijvoet Centre for Biomolecular Research, Department of Chemistry, Faculty of Science, Utrecht University

## Corresponding Authors

**Markus Weingarth**
m.weingarth@uu.nl

**Marc Baldus**
m.baldus@uu.nl

## Citation

Beriashvili, D., Schellevis, R.D., Napoli, F., Weingarth, M., Baldus, M. High-Resolution Studies of Proteins in Natural Membranes by Solid-State NMR. *J. Vis. Exp.* (169), e62197, doi:10.3791/62197 (2021).

## Date Published

March 3, 2021

## DOI

10.3791/62197

## URL

jove.com/video/62197

## Abstract

Membrane proteins are vital for cell function and thus represent important drug targets. Solid-state Nuclear Magnetic Resonance (ssNMR) spectroscopy offers a unique access to probe the structure and dynamics of such proteins in biological membranes of increasing complexity. Here, we present modern solid-state NMR spectroscopy as a tool to study structure and dynamics of proteins in natural lipid membranes and at atomic scale. Such spectroscopic studies profit from the use of high-sensitivity ssNMR methods, i.e., proton-($^1$H)-detected ssNMR and DNP (Dynamic Nuclear Polarization) supported ssNMR. Using bacterial outer membrane beta-barrel protein BamA and the ion channel KcsA, we present methods to prepare isotope-labeled membrane proteins and to derive structural and motional information by ssNMR.

## Introduction

Structural and motional studies of membrane proteins in physiologically relevant environments pose a challenge to traditional structural biology techniques[1]. Modern solid-state nuclear magnetic resonance spectroscopy (ssNMR) methods offer a unique approach for the characterization of membrane proteins[2,3,4,5,6,7] and has long been used to study membrane proteins, including membrane embedded protein pumps[8], channels[9,10,11], or receptors[12,13,14,15]. Technical advances such as ultra-high magnetic fields >1,000 MHz, fast magic angle spinning frequencies >100 kHz, and hyperpolarization techniques[16] have established ssNMR as a powerful method for the study of membrane proteins in environments of ever-increasing complexity from liposomes to cell membranes and even whole cells. For example, DNP has become a powerful tool for such experiments (see reference[17,18,19,20,21,22,23,24,25]). More recently,

$^{1}$H-detected ssNMR offers increasing possibilities to study membrane proteins at high spectral resolution and sensitivity[25,26,27,28,29]. This work highlights two bacterial membrane proteins that are involved in essential functions, i.e., protein insertion and ion transport. The corresponding proteins, BamA[25,30,31,32,33] and KcsA[23,27,28,34,35,36,37,38,39] (or chimeric variants thereof[10,40]) have been examined by ssNMR methods for more than a decade.

A representative protocol for the preparation and ssNMR characterization of bacterially originating membrane proteins is presented here. The different steps of the protocol are shown in **Figure 1**. First, the expression, isotope-labeling, purification, and membrane-reconstitution of BamA is explained. Then, a general workflow for the characterization of the membrane protein by ssNMR is presented; specifically, the assignment of membrane protein backbones using $^{1}$H-detected ssNMR at fast magic angle spinning. Finally, basic setup and acquisition of dynamic nuclear polarization-(DNP)-supported experiments, which significantly boost ssNMR signal sensitivity, are detailed.

## Protocol

### 1. Production of uniformly labeled $^{2}$H, $^{13}$C, $^{15}$N-labeled BamA-P4P5

NOTE: While this protocol requires working with non-pathogenic Gram-negative bacteria, adherence to basic biological safety procedures is a must, namely, wearing safety glasses, lab coats, gloves, and following institutional standard operating procedures for work with microorganisms.

1. Use a single colony of *E. coli* BL 21 Star (DE3) containing the pET11aΔssYaeT plasmid encoding for *E. coli* BamA-P4P5 to inoculate 50 mL of Lysogeny broth supplemented with 50 µg/L of ampicillin.
2. Grow the culture at 37 °C at 200 rpm until an $OD_{600}$ of 0.6 is reached. Spin at 2,000 *x g* for 10 min. Resuspend the pellet in 50 mL of M9 (see **Table 1**) to a maximum $OD_{600}$ of 0.1.

   NOTE: All future growing steps take place at the conditions stated above unless otherwise noted.
3. Grow the culture until $OD_{600}$ of 0.5. Spin at 2,000 *x g* for 10 min at room temperature. Resuspend the pellet in 50 mL of M9 containing 90% $D_2O$ (see **Table 1** for recipe) to a maximum $OD_{600}$ of 0.1. Grow the culture overnight at 30 °C at 200 rpm.
4. Spin down the culture at 2,000 x *g* for 10 min at room temperature. Resuspend the pellet in the prewarmed 50 mL 90% $D_2O$ M9 to a maximum $OD_{600}$ of 0.1. Grow until an $OD_{600}$ of 1.0 is reached.
5. Spin down the culture at 2,000 x *g* for 10 min at room temperature. Prepare 100 mL of 100% $D_2O$ M9 medium with isotope-enriched amounts of non-enriched glucose and ammonium chloride. Resuspend in 100% $D_2O$ M9 medium to a maximum $OD_{600}$ of 0.1. Grow until an $OD_{600}$ of 0.7 is reached.
6. Spin down the culture at 2,000 x *g* for 10 min at room temperature. Discard the supernatant and resuspend the pellet in 500 mL of 100% $D_2O$ M9 medium with isotopes (see **Table 1**) to a maximum $OD_{600}$ of 0.1.
7. Allow the culture to grow until an $OD_{600}$ of 0.6-0.9 is reached. Induce with 1 mM of isopropyl β-D-1-thiogalactopyranoside (IPTG). Express for 4 h and harvest cells at 4,000 x *g* for 15 min at room temperature.

## 2. Purification, refolding, and BamA-P4P5 proteo-liposome formation

NOTE: All the steps of this section should be conducted in a fume hood. Special care must be taken when opening tubes post-centrifugation limits harmful aerosols.

1. Thaw the pellet on ice. Resuspend the pellet in 20 mL of cold Buffer 1. See **Table 2** for the Buffers.
2. Spin down the solution at 4,000 x *g* for 20 min at 4 °C. Resuspend the pellet in 20 mL of cold distilled $H_2O$. Allow the suspension to incubate on ice for 10 min.
3. Spin down the suspension at 4,000 x *g* for 20 min at 4 °C. Resuspend in 10 mL cold Buffer 2 and allow to incubate on ice for 30 min.
4. Supplement the mixture with an additional 10 mL of cold buffer 2 and incubate for a further 30 min on ice. Add 0.5% n-Dodecyl-B-D-Maltoside (DDM) and swirl gently.
5. Sonicate the sample on ice at 13 kHz until vicious-use 10 s long on/off pulses. Spin down at 25,000 x *g* for 20 min at 4 °C. Wash three times with 20 mL of Buffer 3. Centrifuge at 25,000 x *g* for 20 min at 4 ˚C.
6. Resuspend the pellet in 20 mL of Buffer 4. Incubate at 37 °C for 30 min. Sonicate the sample on ice at 13 kHz, until clear-use 10 s long on/off pulses.
7. Spin down the sample at 25,000 x *g* for 20 min at 4 °C. Repeat steps 2.4 to 2.6 omitting addition of protease inhibitor and incubation at 37 °C.
8. Wash the pellet with 20 mL of water and twice with Buffer 3. Spin down at 25,000 x *g* for 20 min at 4 °C. Aliquot the suspension into 1 mL microcentrifuge tubes and spin the microcentrifuge tubes at maximum speed on a bench-top centrifuge for 20 min. Inclusion body purity is assessed by 10% SDS-Page gel, see **Figure 2A**. Expected yield for purified BamA-P4P5 triply ($^2H$,$^{13}C$,$^{15}N$) labeled is 30 mg/L.
9. Solubilize inclusion bodies in 200 µL of Buffer 5 and 300 µL of $H_2O$. Add 6M guanidium chloride (GdnCl). Adjust the volume of microcentrifuge tube to 1 mL with $H_2O$. Vortex the mixture and incubate for 4 h at room temperature. Vortex the microcentrifuge tubes periodically (every 30 min).
10. Spin at 100,000 x *g* for 1 h at 4 °C. Use Beer-Lambert's Law to determine protein concentration by 280 nm. The molar extinction coefficient is 117,120 $M^{-1}cm^{-1}$. If concentration is >100 µM dilute with 1x Buffer 5 with 6 M GdnCl. Rapidly dilute the protein 10x in Buffer 6. Incubate the mixture overnight at room temperature.
    NOTE: For ultracentrifugation, use ultracentrifugation grade 1.5 mL tubes.
11. Determine refolding efficiency using a semi-native SDS-Page gel. Take two 10 µL aliquots from step 2.10 and add 10 µL of Lameili buffer (buffer 8) to each aliquot. Boil one sample for 10 min at 95 °C; leave the other aliquot on ice. Afterwards, run both samples at 14 mA on a 10% SDS-Page gel. The stacking and running portions of the gels lack reducing agent and SDS. Protein staining is achieved using Coomassie dye. The expected results are shown in **Figure 2B**.
12. Spin down the sample at 4,000 x *g* for 20 min at 4 °C. Concentrate the sample to a working volume of 8 mL using a 30 kDa centrifugal filter. Spin the sample at 4,000 x *g* for 20 min at 4 °C. Measure protein absorbance at 280 nm. As in step 2.10, determine the protein concentration.
13. Calculate the amount of lipid required for a 10:1 lipid to protein ratio (LPR-mol/mol). From a chloroform stock,

add the required amount of lipids, as calculated in step 2.12, into a 100 mL round bottom flask (RBF). Evacuate the chloroform from the RBF under a gentle stream of nitrogen. Place RBF on high vacuum for 3 h. Hydrate the lipid film with 1 mL of Buffer 7. Incubate RBF for 10 min at 37 °C.

14. Add the protein mixture (from step 2.12) to the RBF.

15. Dilute the protein/lipid mixture (from step 2.14) to the final volume of 50 mL in the RBF. Use Buffer 7 supplemented with 1x protease inhibitor dissolved in DMSO and incubate for 30 min at 37 °C.

16. Dialyze against 100 volumes of Buffer 7 for 2 weeks (use 12-14 kDa molecular weight cut-off dialysis tubing). For the first 24 h, perform the dialysis at room temperature with addition of fresh Buffer 7 every 8 hrs. Afterwards, change the buffer once daily, and perform dialysis at 4 °C.

## 3. Filling of the ssNMR rotor

1. After step 2.16, centrifuge for 30-60 min at 10,000 x *g* at 4 °C so that a pellet is formed. Remove the supernatant with a pipette.
   NOTE: The technique discussed below has been optimized for a 3.2 mm rotor but is applicable for almost any rotor diameter.

2. Pipette the sample into the rotor and gently spin the same down with a table centrifuge.
   NOTE: Depending on sample consistency, one may either use a densification tool to compact the sample, or a spatula instead of a pipette to put the sample into the rotor.

3. Repeat this process 2-3x until the rotor is filled to the correct height and check if there is enough space for the cap left, as indicated by the marker line on the densification tool. Close the rotor with the cap positioning tool on an even surface. Mark half the bottom edge of the rotor.
   NOTE: New ssNMR rotor generations come with a durable laser mark at the bottom edge for the optical detection of the rotor spinning frequency. Otherwise, the use of a sharpie pen is suggested; as the MAS detector has been optimized specifically for sharpie ink.

4. Use a magnifying glass to check whether the cap is well placed.

## 4. Sample characterization by 2D $^{13}$C- $^{13}$C ssNMR spectroscopy

1. Insert the rotor into the magnet, using the automatic spinning routine of the MAS unit, spin the sample up to the desired MAS frequency between 10 and 20 kHz MAS while cooling the sample to 270 K set temperature. Tune and match the $^{1}$H and $^{13}$C channels.
   NOTE: For the choice of the MAS frequency, avoid accidentally matching the chemical shift distance between the spectral Cα region and the Carbonyl carbon region to the spinning frequency, i.e., avoid the first order rotational resonance condition[41].

2. Optimize a $^{1}$H-$^{13}$C cross-polarization[42] (CP) experiment by varying the rf power on the proton channel from 25-80 kHz. Typical parameters are 45 kHz rf power on $^{13}$C, 80-100 kHz heteronuclear $^{1}$H-decoupling[43] during acquisition, 1.8-2.0 s recycle delay, and 64 scans.
   1. Optimize the CP contact time for maximal signal sensitivity on the aliphatic carbons.
   2. Determine $^{1}$H 90° pulse length in the $^{13}$C-CP experiment by multiplying the starting pulse by

four, i.e., by optimizing a 360° pulse, and vary the length until the signal has disappeared. Include a rectangular pulse directly after the CP transfer and optimize the $^{13}$C 90° pulse length analogously.

3. Run a 2D $^{13}$C-$^{13}$C proton-driven spin diffusion (PDSD)-type experiment such as PARIS with 30 ms magnetization transfer time to detect intra-residual correlations and gauge the sample quality. Transfer the power-levels, the contact time, and 90° pulse lengths from the previously optimized $^{13}$C-CP experiment. Use an acquisition time of 4-6 ms in the indirect dimension. Process the spectrum with squared sin bell functions (QSIN) or, for insensitive samples, exponential line broadening in both dimensions.

4. Extract slices of isolated cross-peaks and determine the linewidth at half heights. A linewidth between ~0.3-1.0 $^{13}$C ppm is indicative of a well-ordered sample, ideal for ssNMR characterization, whereas a linewidth above 1.0 $^{13}$C ppm is indicative of conformational heterogeneity that may compromise ssNMR characterization. The 2D CC PARIS spectrum of BamA shown in **Figure 3A** is an example of a well-ordered protein that gives high-quality spectra.

## 5. Backbone assignment by $^{1}$H-detected 3D ssNMR spectroscopy

1. Acquisition of 2D NH spectral fingerprints

    1. Fill the sample in a 1.3 mm rotor, as described above. Insert the rotor into the magnet, spin the sample to 10-20 kHz MAS and cool the sample to 240-250 K set temperature or lower, depending on the specifications of the ssNMR probehead. Use the MAS unit interface to increase the MAS frequency gradually in steps of 5 kHz to 60 kHz MAS.

    2. Optimize the CP amplitudes, contact times, and 90° pulse lengths in $^{13}$C- and $^{15}$N CP experiments. Use amplitudes around 30-50 or 70-100 kHz on the heteronuclear channels and vary the amplitude on the $^{1}$H-channel from 80-180 kHz. Use a recycling delay of 0.7-1.2 s, along with 15 kHz low-power heteronuclear proton decoupling[44]. Also, see reference[45] for further practical details on how to set up CP ssNMR experiments.

    3. Acquire a 2D NH experiment to gauge the $^{1}$H-resolution. Transfer the $^{15}$N-CP parameters and use approximately 15 and 25 ms acquisition time in the direct and indirect dimensions. For the first $^{1}$H to $^{15}$N CP transfer, use the previously optimized contact time. For the $^{15}$N to $^{1}$H backtransfer, use 0.7-1.0 ms contact time to minimize interresidual magnetization transfer.

    4. Use 50-250 ms water MISSISSIPPI suppression[46], dependent on sample water content. Process the spectrum with squared sin bell functions (QSIN) in both dimensions. Extract slices of isolated cross-peaks and determine the linewidth at half heights. An example for a high-quality 2D NH spectrum[25] is shown for membrane-embedded BamA-P4P5 in **Figure 3B**.

2. **Backbone assignments**

    1. Optimize a 1D $^{15}$N to $^{13}$Cα specific CP experiment[47]. Place the $^{13}$C carrier in the middle of the Cα region around 55 ppm. Use a $^{13}$C rf

amplitude of 20 kHz and vary the $^{15}N$ amplitude from 35 to 45 kHz for maximal transfer to the Cα signals and minimal transfer to the carbonyl signals. Optimize the contact time from 3 to 10 ms in increments of 1 ms.

2. Run a 3D CαNH experiment. Transfer all CP amplitudes, contact times, and pulse lengths from the previously optimized steps. Use approximately 10 ms and 30 ms in the indirect and direct acquisition dimensions. Process the spectrum with squared sin bell functions (QSIN) in all three dimensions.

3. Optimize a 1D Cα to CO DREAM magnetization transfer[48]. Start with a $^{15}N$ to $^{13}Cα$ specific CP transfer. Then, transfer the magnetization from Cα to CO using a spin lock on the $^{13}C$ channel. Vary the *rf* amplitude from 20 to 35 kHz for optimal transfer. Optimize the transfer time from 4 to 10 ms.

4. Run a 3D Cα(CO)NH experiment. Transfer all rf amplitudes, contact times, and pulse lengths from the previously optimized steps. Use approximately 10 ms and 30 ms in the indirect and direct acquisition dimensions. Process the spectrum with squared sin bell functions (QSIN) in all three dimensions.

5. Repeat and adapt steps 1-4 for the analogous 3D CONH and CO(Cα)NH experiments. Use this quartet of 3D experiments for sequential Cα and CO walks to assign the protein backbone, as shown on the example of KcsA in **Figure 4**[28].

## 6. Protein dynamics by $^{1}H$-detected ssNMR spectroscopy

1. For $^{15}N$ $T_1$ studies, use the previously optimized 2D NH experiment at 60 kHz MAS and include a delay after the first $^{1}H$ to $^{15}N$ cross-polarization step. Acquire a series of 2D NH experiments and vary the delay from 0 to 16 s using steps of, e.g., 0, 2, 4, 8, and 16 s.

2. Plot the normalized intensities for resolved signals as a function of the increasing delay time. Fit the $T_1$ decay to single exponentials according to $y = exp^{(-x/T1)}$, with y being the signal intensity at decay time x.

3. Analogously, for $^{15}N$ $T_{1rho}$ studies, include a spin-lock pulse in the pulse program on the $^{15}N$ channel with an rf amplitude between 15-20 kHz after the first $^{1}H$ to $^{15}N$ cross-polarization step[26,49]. Acquire a series of 2D NH experiments and vary the delay from 0 to 150 ms and fit the $T_{1rho}$ decay of resolved signals to single exponentials. Illustrative $^{15}N$ $T_{1rho}$ data is shown for membrane-embedded $K^+$ channels in **Figure 5**[27,28].

## 7. Dynamic nuclear polarization

NOTE: The following preparative steps relate to the use of a commercial DNP setups using 3.2 mm sapphire MAS rotors (**Figure 6**)[20]. Use of the zirconia rotors or other DNP equipment may lead to lower DNP signal enhancements.

1. Resuspend membrane protein pellet (from step 3.1) in 50 µL of deuterated DNP buffer (60% (v/v) deuterated d8- and glycerol, and 15 mM AMUPol[50]. For experiments at 800 MHz, we recommend using 10 mM NATriPOL-3[51]. Also see reference[52] for further practical aspects to DNP ssNMR experiments.

2. Centrifuge for 10-20 min at 100,000 x *g* at 4 °C so that a pellet is formed. Remove the supernatant with a pipette.

3. Precool the centrifugal adaptor and the 3.2 mm sapphire MAS rotor components to <4 °C. The following steps

(7.4-7.7) need to be done as quickly as possible to prevent the DNP agents from getting reduced.

4. Place the 3.2 mm sapphire rotor in the centrifuge adapter and fill it with the suspension of proteo-liposomes from step 7.2.

5. Pipette the resuspended membrane protein sample against the inner wall of the rotor carefully using a 200 µL pipette tip. Allow the solution to slide down to the bottom of the rotor. Ensure that air bubbles are not formed.

6. Spin down the sample in the rotor for 5-10 mins at 4,500 x *g* at 4 °C. Remove the supernatant containing excess DNP juice by pipetting it out carefully without disrupting the cell pellet. Repeat steps 6.4-6.6 until the rotor is full.

7. Carefully position the polytetrafluoroethylene (PTFE) spacer using the spacer screw on top of the rotor.

8. Place the rotor, cap side down in a rotor plunger[53] and plunge the rotor into liquid nitrogen. Allow at least 30-60 s for the rotor and the sample to freeze.

9. Start up the heat exchanger unit and cool down the DNP probe to ~90K.

10. Set the MAS unit to **Manual mode** and set the variable temperature (VT) to 135 l/h and bearing and drive gas flows to ~6 l/h.

11. Engage **Eject** on the MAS console.

12. Transfer the frozen sample from Step 7.8 from the liquid N2 into the sample catcher and place it in the probe (also see reference[53]).

13. Manually increase the probe bearing pressure (Bp) to ~500 mbar before engaging the "Insert". This is advisable for stable and safe spinning of the rotor.

14. Increase MAS rate to the desired value using the procedure described in reference[53].

15. Check for DNP enhancements with and without microwaves using a standard 1D CP experiments (also see, e.g., reference[51,54]) (**Figure 7**) before proceeding with multidimensional experiments, e.g., 2D CC experiments described in section 3 of this article.

## Representative Results

**Figure 2** shows representative gels for inclusion body purity (Panel A) and refolding of inclusion bodies (Panel B3). **Figure 2** confirms the successful purification of $^{13}C$,$^{15}N$-labeled BamA-P4P5.

**Figure 3A** shows a typical 2D $^{13}C$-$^{13}C$ spectrum of a well-ordered membrane protein, and **Figure 3B** shows a typical, high-quality 2D $^{15}N^{1}H$ spectrum of a perdeuterated membrane protein[25]. Note that this membrane protein expressed as inclusion bodies, so that the transmembrane part is also accessible by perdeuteration. For membrane proteins that do not express in inclusion bodies, one usually needs to employ $H_2O$-based growth media[27,55,56,57].

**Figure 4** exemplifies how to assign the backbone of membrane proteins using $^{1}H$-detected 3D experiments[28]. **Figure 5** demonstrates the powerof ssNMR relaxation measurements that can provide detailed, site-resolved information on the dynamics of membrane proteins[28,49].

Eventually, **Figure 6** and **Figure 7** illustrate how DNP can boost the sensitivity of ssNMR experiments of membrane-embedded proteins[25]. **Figure 6** shows high-resolution DNP-supported ssNMR information on the structure of the outer-membrane protein BamA.

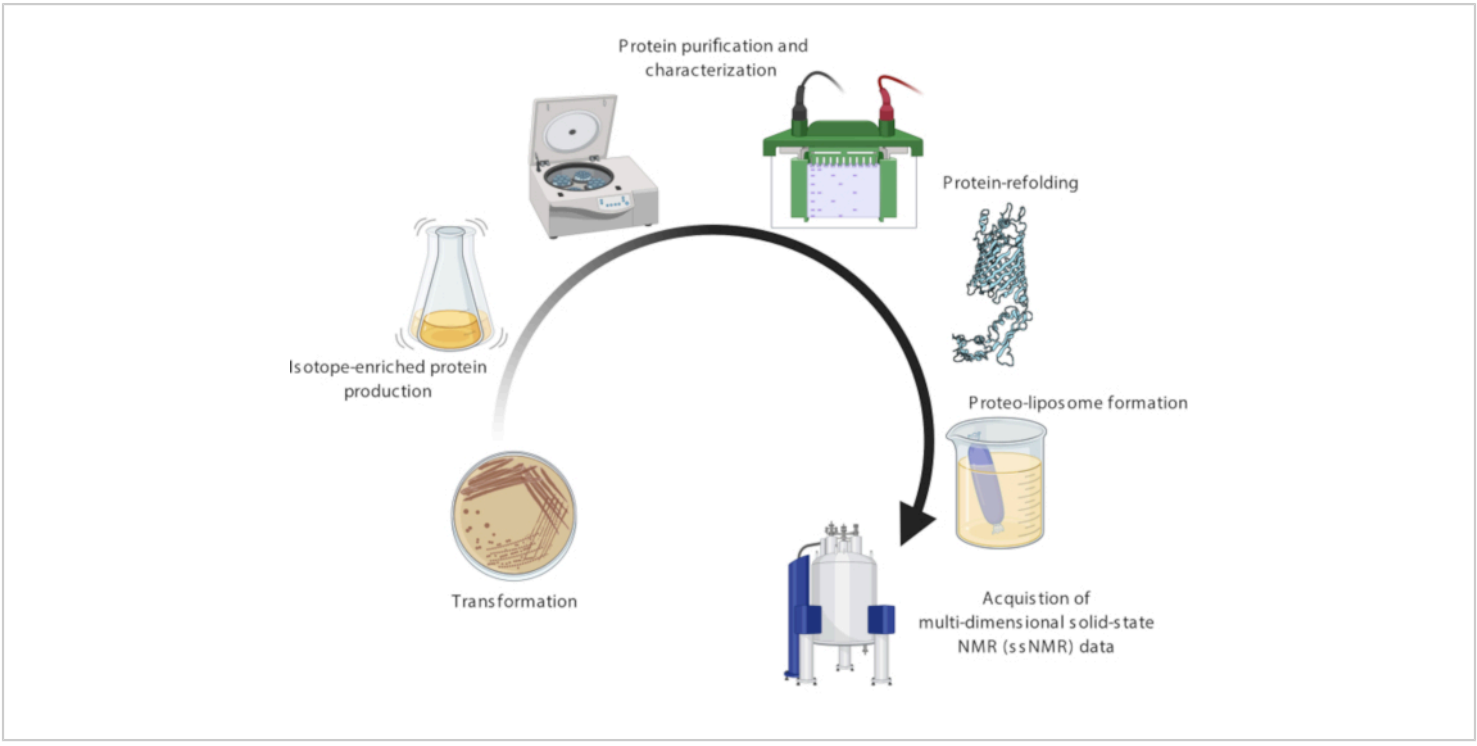


**Figure 1: Experimental methodology for atomic-level multidimensional solid-state nuclear magnetic resonance (ssNMR) studies of membrane proteins embedded in native-membrane environments.** Specifically, the workflow details robust procedures for membrane protein production, purification, refolding, proteo-liposomes formation, and most crucially setup/acquisition/analysis of cutting-edge multidimensional ssNMR spectra. Please click here to view a larger version of this figure.

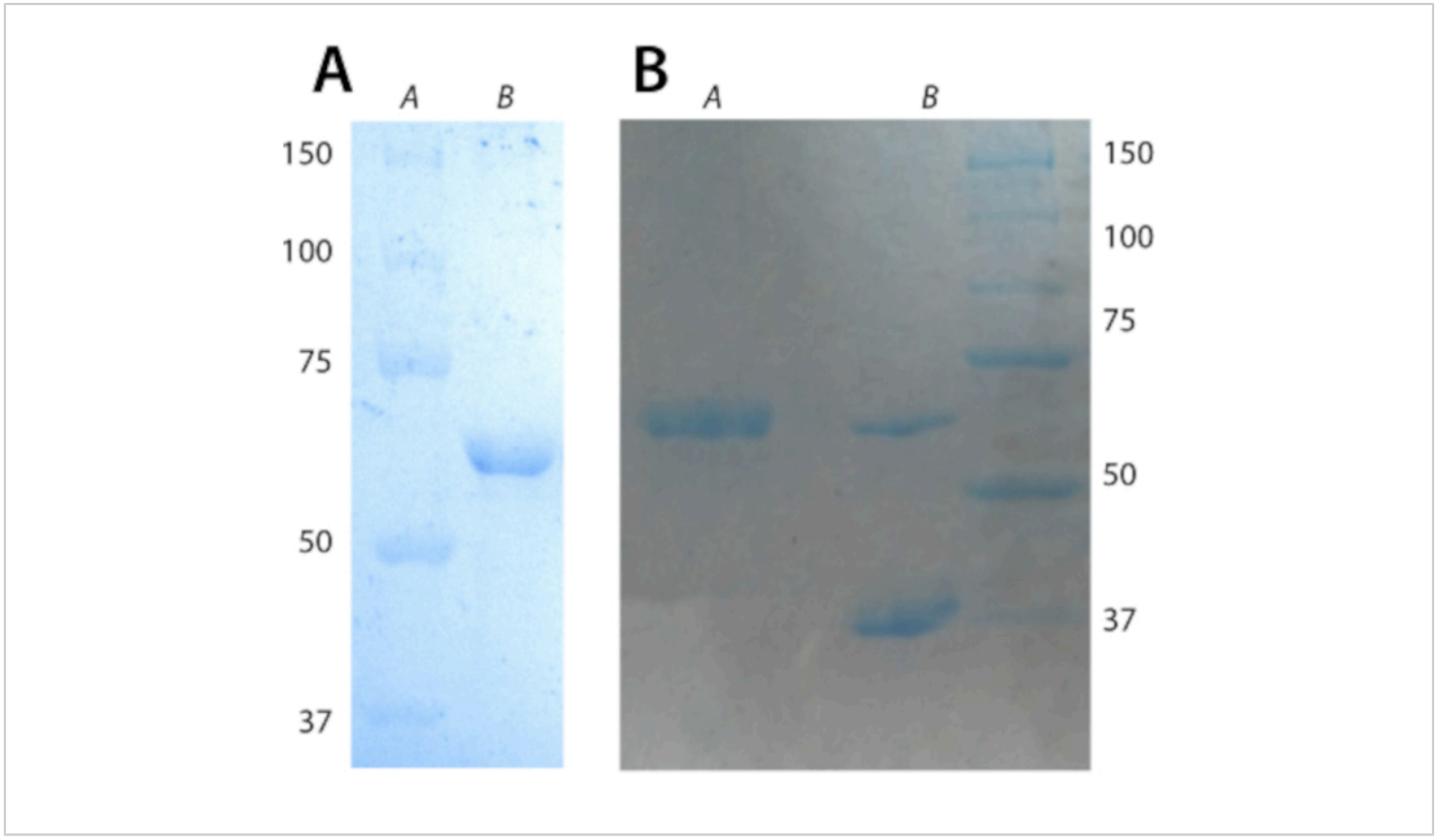


**Figure 2: Representative gels for inclusion body purity and refolding.** (**A**) 10% SDS-Page gel of BamA-P4P5 inclusion bodies. Lane A has the molecular weight ladder; Lane B has BamA-P4P5 inclusion bodies. The expected molecular weight of BamA-P4P5 is 61.1 kDa. (**B**) 10% SDS-page semi native gel for assessing BamA-P4P5 refolding efficiency. Lane A contains the boiled sample; as expected, it migrates to the molecular weight of 61.1 kDa. Lane B contains the un-boiled sample; the top band is protein that has remained unfolded and the bottom band near 37 kDa is the folded population. The folding efficiency can be determined using image analysis software-in this specific case, folding efficiency is >70%. Please click here to view a larger version of this figure.

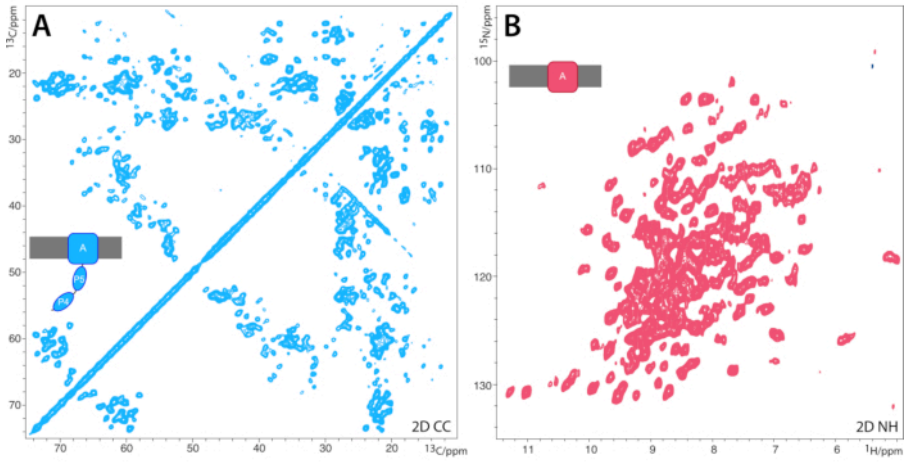


**Figure 3: Representative 2D $^{13}C^{13}C$ PARIS and $^{1}H$-detected NH spectra for BamA-P4P5 proteo-liposomes.** (**A**) 2D $^{13}C^{13}C$ PARIS spectrum of $^{13}C,^{15}N$-labeled BamAP4P5 in liposomes. The spectrum was acquired at 700 MHz ($^{1}H$-frequency) magnetic field using 13 kHz MAS and a $^{13}C^{13}C$ magnetization transfer time of 30 ms. (**B**) $^{1}H$-detected 2D NH spectrum of the $^{2}H,^{13}C,^{15}N$-labeled transmembrane part of BamA in liposomes. The spectrum was acquired at 800 MHz ($^{1}H$-frequency) and 60 kHz MAS. This figure has been modified from reference[25]. Please click here to view a larger version of this figure.

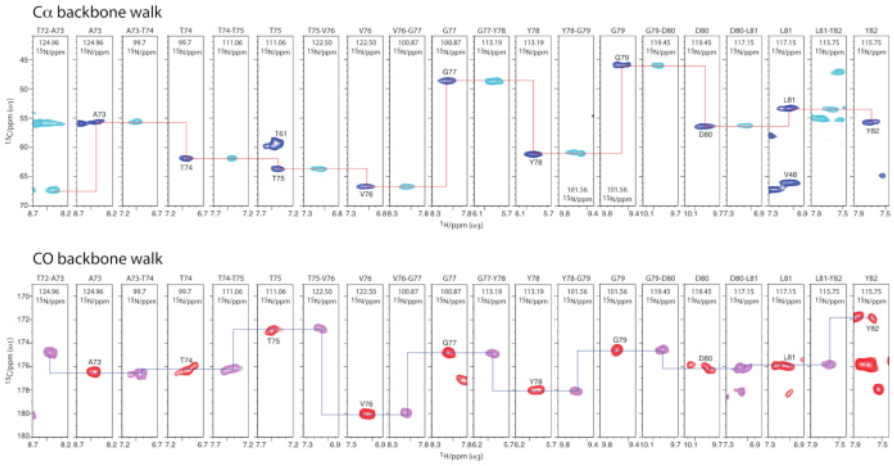


**Figure 4: Sequential ssNMR assignments of membrane-embedded ion channels with $^{1}$H-detected 3D experiments.** Upper panel: Cα-Cα+1 backbone walk showing full connectivity for residues T72-Y82 in KcsA mutant E71A. Dark blue signals show CαH planes from a 3D CαNH experiment, cyan CαH planes were taken from a 3D CαcoNH experiment. Lower panel: CO-1-CO backbone walk showing full connectivity for residues T72-Y82 in E71A. Magenta signals show COH planes from a 3D CONH experiment, red COH planes were taken from a 3D COcαNH experiment. This figure has been modified from reference[28]. Please click here to view a larger version of this figure.

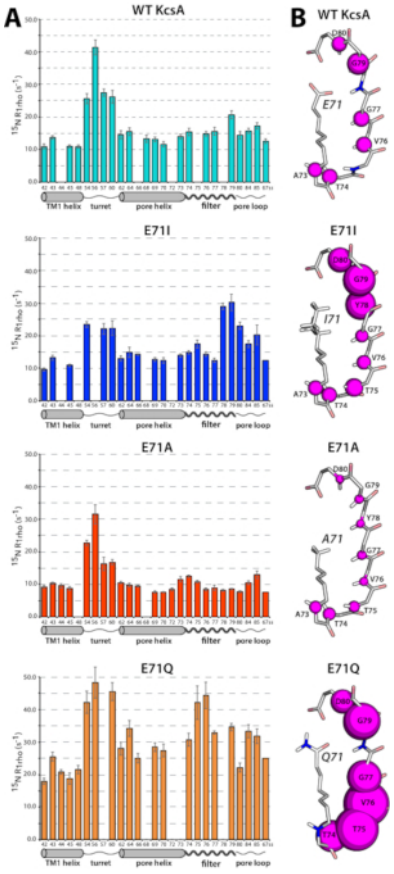


**Figure 5: SSNMR $^{15}$N $T_{1rho}$ data reveal differential dynamics in membrane-embedded point-mutants of the bacterial potassium channel KcsA.** (**A**) $^{15}$N rotating frame ssNMR relaxation rates ($R_{1rho}$) that report on slow molecular motions in WT KcsA (cyan), E71A (red), E71I (blue), and E71Q (orange) measured at 700 MHz and 58 kHz MAS. The error bars show the standard error of the fit. (**B**) Illustration of the site-resolved selectivity filter dynamics. The size of the magenta spheres represents the $R_{1rho}$ relaxation rates. This figure has been modified from reference[28]. Please click here to view a larger version of this figure.

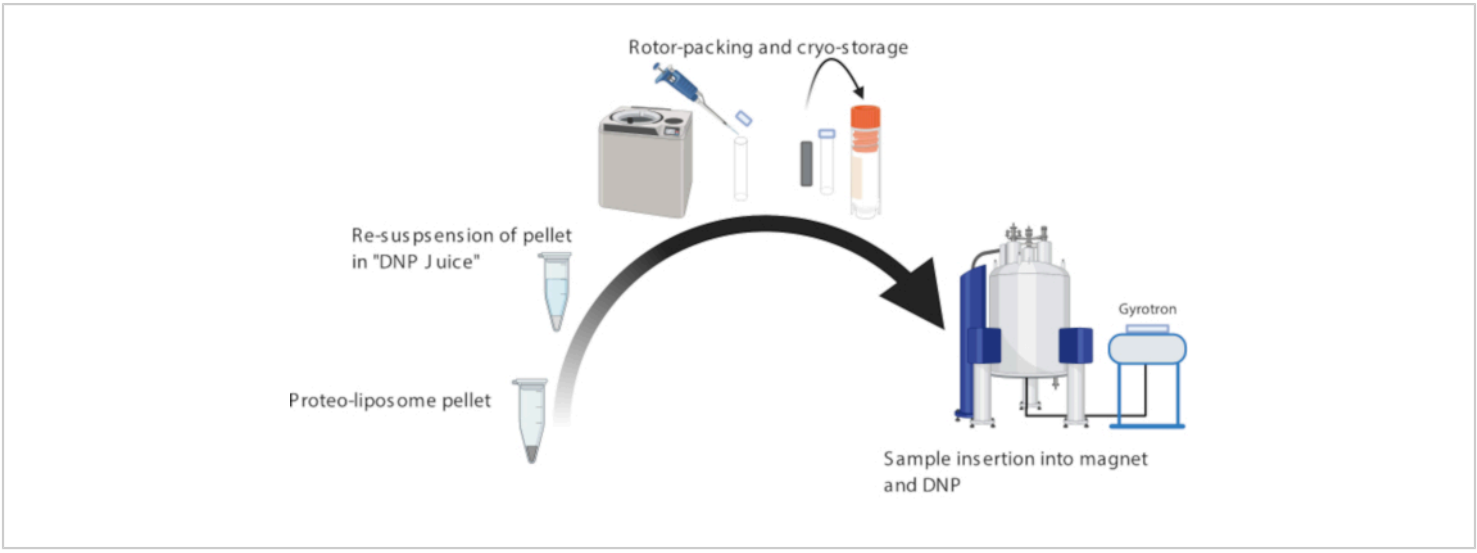


**Figure 6: Preparation of proteo-liposomes for dynamic nuclear polarization (DNP) NMR experiments.** Important steps are highlighted, including resuspension of proteo-liposomes in DNP juice, packing the sample into a sapphire rotor, and ultimately execution of DNP measurements. Please click here to view a larger version of this figure.

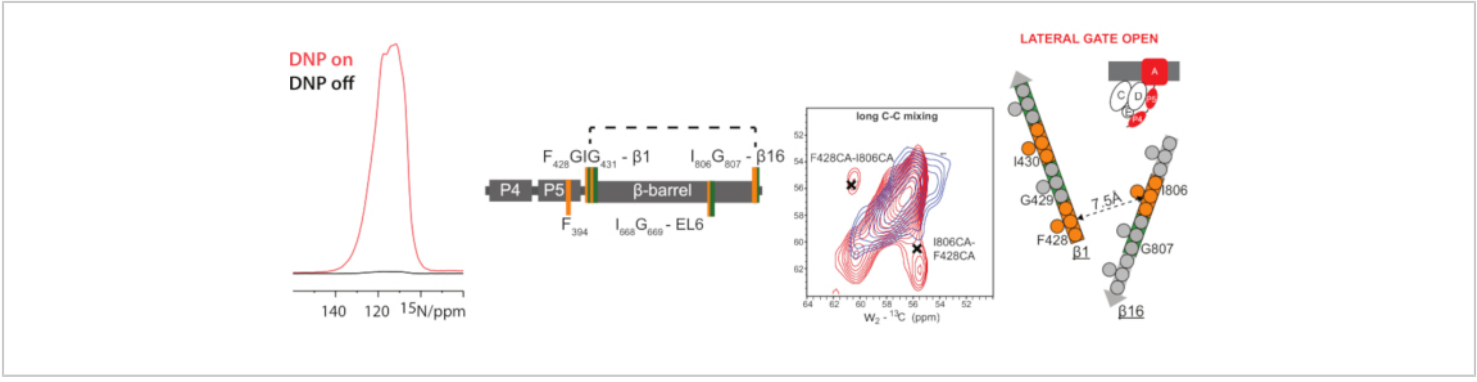


**Figure 7: DNP spectra of $^{13}$C and $^{15}$N-labeled BamA-P4P5.** Left: A DNP signal enhancement of about 110 could be obtained for membrane-embedded $^{13}$C,$^{15}$N-IFG-labeled BamAP4P5 using a 400 MHz/263 GHz DNP system. Right: Close-up of the Cα-Cβ region of the DNP enhanced $^{15}$N-edited carbon-carbon correlation experiment[58] using a long (1 s) mixing time, measured on $^{13}$C,$^{15}$N-IFG-labeled BamAP4P5, in the presence (red spectrum) and absence (blue spectrum) of unlabeled BamCDE. Crosses are the tentative assignments for the residues targeted by these experiments. Schematic representation of the correlations observed between β-strand 1 and 16 in $^{15}$N-edited $C_XC_X$ DNP spectra for the case of a lateral gate open. The distance between Cα residues of the closest residue in β1 to the I806 of β16 is indicated. This figure has been modified from reference[25]. Please click here to view a larger version of this figure.

| Chemical | **Amount/Volume for 1L of Medium** |
|---|---|
| Disodium phosphate | 6.0 g |
| Monopotassium phosphate | 3.0 g |
| Sodium Chloride | 0.5 g |
| Ammonium Chloride – both nitrogen-15 enriched and not enriched | 0.5 g |
| Magnesium sulphate (1 M) | 2 mL |
| Calcium dichloride (1 M) | 10 µL |
| Iron sulphate (0.01 M) | 1 mL |
| Isotope enriched glucose* | 2 g |
| Glucose | 5 g |
| Thiamine (0.5 mg/mL) | 10 mL |
| Micronutrients | 1 mL |
| Vitamin Supplements | 1 mL |
| Ampicillin (50 mg/mL) | 1 mL |

**Table 1: M9 minimal medium recipe.** The medium can be made up in $H_2O$ or varying amounts of $D_2O$ as directed by the protocol. *In case of perdeuterated protein production D-Glucose-$^{13}C_6$,1,2,3,4,5,6,6-$d_7$ is used.

| Chemical | Final Concentration |
|---|---|
| **Buffer 1** | |
| Tris-HCl pH 8.0 | 50 mM |
| EDTA | 40 mM |
| **Buffer 2** | |
| Tris-HCl pH 8.0 | 50 mM |
| EDTA | 40 mM |
| Lysozyme | .2 mg/mL |
| Sucrose | 25% |
| **Buffer 3** | |
| Tris-HCl pH 8.0 | 10 mM |
| **Buffer 4** | |
| Tris-HCl pH 8.0 | 10 mM |
| $MgCl_2$ | 2 mM |
| Benzonase (>90%) | 40 units |
| Sucrose | 25% |
| DDM | 0.10% |
| Protease inhibitor cocktail in DMSO | 1x |
| **Buffer 5** | |
| Tris-HCl pH 8.0 | 100 mM |
| Glycine | 500 mM |
| **Buffer 6** | |
| Sodium Phosphate pH 7 | 50 mM |
| lauryl-dimethylamine oxide (LDAO) | 1% |
| Protease inhibitor cocktail in DMSO | 1x |
| **Buffer 7** | |
| Sodium Phosphate pH 7 | 20 mM |

| | |
|---|---|
| $MgCl_2$ | 5 mM |
| **Buffer 8** | |
| Tris-HCl pH 6.8 | 62.5 mM |
| Sodium dodecyl sulfate | 0.10% |
| Glycerol | 10% |
| Bromophenol blue | 0.00% |

**Table 2: Buffers used for the sample preparation of membrane embedded BamA.**

| Chemical | Concentration (mol/L) |
|---|---|
| Ammonium molibdate | $3 \times 10^{-6}$ |
| Boric acid | $4 \times 10^{-4}$ |
| Cobalt chloride | $3 \times 10^{-5}$ |
| Copper sulphate | $1 \times 10^{-5}$ |
| Manganese chloride | $8 \times 10^{-5}$ |
| Zinc chloride | $1 \times 10^{-5}$ |
| **Note:** The stock can be made up in water or varying amounts of $D_2O$ as directed by the protocol. | |

**Table 3: Micronutrients stock (1,000x).** The stock can be made up in water or varying amounts of $D_2O$ as directed by the protocol.

| Chemical | Amount (mg) for 100 mL of Supplement |
|---|---|
| D-Biotin | 100 |
| Choline chloride | 50 |
| Folic acid | 50 |
| Myoinositol | 100 |
| Nicatinamide | 50 |
| Panthotenic acid | 50 |
| Pyridoxal-HCl | 50 |
| Riboflavin | 5 |
| Thiamine-HCl | 50 |
| **Note:** The supplement can be made up in $H_2O$ or varying amounts of $D_2O$ as directed by the protocol. | |

**Table 4: Vitamin Supplement (1,000x) for 100 mL.** The supplement can be made up in $H_2O$ or varying amounts of $D_2O$ as directed by the protocol.

## Discussion

Membrane proteins are key players in the regulation of vital cellular functions both in prokaryotic and eukaryotic organisms; thus, understanding their action mechanisms at atomic levels of resolution is of vital importance. The existing structural biology techniques have pushed scientific understanding of membrane proteins quite far but have heavily relied on experimental data gathered from in vitro systems devoid of membranes. In this article, an experimental approach is presented that allows to obtain atomistic insight into the structure and function of two bacterial membrane-proteins embedded in native-like membrane by utilizing cutting-edge solid-state NMR techniques, namely, fast-MAS and DNP. This method is broadly applicable to other bacterial membrane proteins.

The protocol begins by describing a robust methodology to produce and purify triply isotope labeled BamA in high yield and purity **(Figure 2A)** -other stable-isotope labeling schemes can be employed. The purification protocol makes use of synergy between surfactant activity and sonication to remove cellular debris from BamA inclusion bodies. The subsequent refolding sees formation of BamA-LDAO micelles (**Figure 2B**). Further addition of lipids and dialysis aids in the removal of LDAO and residual surfactant molecules thereby facilitating formation of proteo-liposomes suitable for solid-state NMR studies. The formation of proteo-liposomes is a crucial step and must be done with adherence to the buffer exchange schedule detailed above. This is mandatory for a successful preparation.

The acquisition of 2D spin diffusion-based CC spectra (**Figure 3A**) of membrane proteins is routine and often

among the first experiments conducted to gauge the sample's quality and secondary structure content. By using long CC mixing times, these experiments can also be conveniently used to derive structural information. Note that spin diffusion transfer efficacy inversely scales with the MAS frequency. Hence, longer mixing times are required with increasing MAS frequency.

If the membrane-protein is grown in $D_2O$-based buffers as in the representative example of **Figure 3B**, it is necessary to back-exchange the amino-protons in $H_2O$-based buffers afterwards[59]. This may prevent the detection of the water-inaccessible transmembrane-part. This limitation can be overcome by the use of dedicated $H_2O$-based growth media[27] or fully-protonated membrane proteins in combination with MAS frequencies above 100 kHz[55,56,57,60].

Spectral assignments of small membrane proteins can be conveniently performed with the quartet of $^1$H-detected 3D experiments that is shown in **Figure 4** for the selective filter of the $K^+$ channel E71A KcsA[28]. This quartet can be supplemented by a 3D CαCαNH experiment or 2D CC experiments to obtain sidechain information that simplifies the assignments. For larger membrane proteins, the use of 4D or higher order experiments is necessary to disambiguate the assignments. These spectra are usually acquired with dedicated non-uniform sampling strategies in order to shorten experimental time.

Detailed relaxation data is shown in **Figure 5** for the $K^+$ channel KcsA and three KcsA point mutants with different gating behaviors, hence correlation membrane protein dynamics to function[28]. For example, compared to the WT KcsA channel, the constitutively active mutant E71A shows a striking rigidification, and the so-called "flicker" mutant E71Q shows a marked increase in global protein dynamics. For relaxation measurements, a high sensitivity is indispensable because signals toward the end of the relaxation series also need to be acquired with robust signal-to-noise ratios.

The spectacular advantages of DNP are shown in **Figure 6** and **Figure 7**. DNP can strongly improve sensitivity in ssNMR experiments that enable otherwise infeasible experiments[27,61,62,63]. In **Figure 7B**, we utilized DNP to probe residue-specific, through-space contacts in a membrane-embedded BamA (547 residues)-Bam CDE complex. A combination of amino-acid specific labeling and DNP-supported $^{15}$N-edited $^{13}$C-$^{13}$C correlation spectroscopy[58] allows to probe through-space contacts between α-strands 1 and 16, suggesting the so-called lateral gate that is critical for function (see, e.g., reference[64]) is open.

In the future, we expect modern solid-state NMR methods to continue to play a major role for structural and dynamical studies of membrane proteins, especially in complex media such as cellular preparations and whole cells.

## Disclosures

The authors have nothing to disclose.

## Acknowledgments

This work is part of the research programs ECHO, TOP, TOP-PUNT, VICI, and VIDI with project numbers 723.014.003, 711.018.001, 700.26.121, 700.10.443, and 718.015.00, which are financed by the Dutch Research Council (NWO).

## References

1. Weingarth, M., Baldus, M. Solid-state NMR-based approaches for supramolecular structure elucidation.

*Accounts of Chemical Research.* **46** (9), 2037-2046 (2013).

2. Kaplan, M., Pinto, C., Houben, K., Baldus, M. Nuclear magnetic resonance (NMR) applied to membrane-protein complexes. *Quarterly Reviews of Biophysics.* **49**, e15 (2016).
3. Brown, L. S., Ladizhansky, V. Membrane proteins in their native habitat as seen by solid-state NMR spectroscopy. *Protein Science.* **24** (9), 1333-1346 (2015).
4. Ladizhansky, V. Applications of solid-state NMR to membrane proteins. *Biochimica Et Biophysica Acta. Proteins and Proteomics.* **1865** (11 Pt B), 1577-1586 (2017).
5. Hong, M., Zhang, Y., Hu, F. H. Membrane protein structure and dynamics from NMR spectroscopy. *Annual Review of Physical Chemistry.* **63**, 1-24 (2012).
6. Shahid, S. A. et al. Membrane-protein structure determination by solid-state NMR spectroscopy of microcrystals. *Nature Methods.* **9** (12), 1212-1217 (2012).
7. Wang, S. L. et al. Solid-state NMR spectroscopy structure determination of a lipid-embedded heptahelical membrane protein. *Nature Methods.* **10** (10), 1007-1012 (2013).
8. Herzfeld, J., Lansing, J. C. Magnetic resonance studies of the bacteriorhodopsin pump cycle. *Annual Review of Biophysics and Biomolecular Structure.* **31** (1), 73-95 (2002).
9. Ketchem, R. R., Hu, W.,Cross, T. A. High-resolution conformation of gramicidin A in a lipid bilayer by solid-state NMR. *Science.* **261** (5127), 1457-1460 (1993).
10. Lange, A. et al. Toxin-induced conformational changes in a potassium channel revealed by solid-state NMR. *Nature.* **440** (7086), 959-962 (2006).
11. Cady, S. D. et al. Structure of the amantadine binding site of influenza M2 proton channels in lipid bilayers. *Nature.* **463** (7281), 689-692 (2010).
12. Park, S. H. et al. Structure of the chemokine receptor CXCR1 in phospholipid bilayers. *Nature.* **491** (7426), 779-783 (2012).
13. Luca, S. et al. The conformation of neurotensin bound to its G protein-coupled receptor. *Proceedings of the National Academy of Sciences of the United States of America.* **100** (19), 10706-10711 (2003).
14. Joedicke, L. et al. The molecular basis of subtype selectivity of human kinin G-protein-coupled receptors. *Nature Chemical Biology.* **14** (3), 284-290 (2018).
15. Krug, U. et al. The conformational equilibrium of the neuropeptide Y2 receptor in bilayer membranes. *Angewandte Chemie (International Edition in English).* ***59***. (52), 23854-23861 (2020).
16. Maly, T. et al. Dynamic nuclear polarization at high magnetic fields. *Journal of Chemical Physics.* **128** (5) (2008).
17. Bajaj, V. S., Mak-Jurkauskas, M. L., Belenky, M., Herzfeld, J., Griffin, R. G. Functional and shunt states of bacteriorhodopsin resolved by 250 GHz dynamic nuclear polarization-enhanced solid-state NMR. *Proceedings of the National Academy of Sciences of the United States of America.* **106** (23), 9244-9249 (2009).
18. Linden, A. H. et al. Neurotoxin II bound to acetylcholine receptors in native membranes studied by dynamic

nuclear polarization NMR. *Journal of the American Chemical Society.* **133** (48), 19266-19269 (2011).

19. Ong, Y. S., Lakatos, A., Becker-Baldus, J., Pos, K. M., Glaubitz, C. Detecting substrates bound to the secondary multidrug efflux pump EmrE by DNP-enhanced solid-state NMR. *Journal of the American Chemical Society.* **135** (42), 15754-15762 (2013).
20. Koers, E. J. et al. NMR-based structural biology enhanced by dynamic nuclear polarization at high magnetic field. *Journal of Biomolecular NMR.* **60** (2-3), 157-168 (2014).
21. Becker-Baldus, J. et al. Enlightening the photoactive site of channelrhodopsin-2 by DNP-enhanced solid-state NMR spectroscopy. *Proceedings of the National Academy of Sciences of the United States of America.* **112** (32), 9896-9901 (2015).
22. Kaplan, M. et al. EGFR dynamics change during activation in native membranes as revealed by NMR. *Cell.* **167** (5), 1241-1251 (2016).
23. Visscher, K. M. et al. Supramolecular organization and functional implications of K+ channel clusters in membranes. *Angewandte Chemie (International Edition in English).* **56** (43), 13222-13227 (2017).
24. Joedicke, L. et al. The molecular basis of subtype selectivity of human kinin G-protein-coupled receptors. *Nature Chemical Biology.* **14**, 284 (2018).
25. Pinto, C. et al. Formation of the beta-barrel assembly machinery complex in lipid bilayers as seen by solid-state NMR. *Nature Communications.* **9** (2018).
26. Good, D. B. et al. Conformational dynamics of a seven transmembrane helical protein Anabaena Sensory Rhodopsin probed by solid-state NMR. *Journal of the American Chemical Society.* **136** (7), 2833-2842 (2014).
27. Medeiros-Silva, J. et al. (1) H-detected solid-state NMR studies of water-inaccessible proteins in vitro and in situ. *Angewandte Chemie (International Edition in English).* **55** (43), 13606-13610 (2016).
28. Jekhmane, S. et al. Shifts in the selectivity filter dynamics cause modal gating in K(+) channels. *Nature Communications.* **10** (1), 123 (2019).
29. Schubeis, T., Le Marchand, T., Andreas, L. B., Pintacuda, G. 1H magic-angle spinning NMR evolves as a powerful new tool for membrane proteins. *Journal of Magnetic Resonance.* **287**, 140-152 (2018).
30. Sinnige, T. et al. Solid-state NMR studies of full-length BamA in lipid bilayers suggest limited overall POTRA mobility. *Journal of Molecular Biology.* **426** (9), 2009-2021 (2014).
31. Sinnige, T. et al. Insight into the conformational stability of membrane-embedded BamA using a combined solution and solid-state NMR approach. *Journal of Biomolecular NMR.* **61** (3-4), 321-332 (2015).
32. Sinnige, T. et al. Conformational plasticity of the POTRA 5 domain in the outer membrane protein assembly factor BamA. *Structure.* **23** (7), 1317-1324 (2015).
33. Renault, M., Bos, M. P., Tommassen, J., Baldus, M. Solid-state NMR on a large multidomain integral membrane protein: the outer membrane protein assembly factor BamA. *Journal of the American Chemical Society.* **133** (12), 4175-4177 (2011).
34. Doyle, D. A. et al. The structure of the potassium channel: molecular basis of K+ conduction and selectivity. *Science.* **280** (5360), 69-77 (1998).

35. Wylie, B. J., Bhate, M. P., McDermott, A. E. Transmembrane allosteric coupling of the gates in a potassium channel. *Proceedings of the National Academy of Sciences of the United States of America.* **111** (1), 185-190 (2014).

36. Xu, Y., Zhang, D., Rogawski, R., Nimigean, C. M., McDermott, A. E. Identifying coupled clusters of allostery participants through chemical shift perturbations. *Proceedings of the National Academy of Sciences of the United States of America.* **116** (6), 2078-2085 (2019).

37. van der Cruijsen, E. A. W., Prokofyev, A. V., Pongs, O., Baldus, M. Probing conformational changes during the gating cycle of a potassium channel in lipid bilayers. *Biophysical Journal.* **112** (1), 99-108 (2017).

38. Varga, K., Tian, L., McDermott, A. E. Solid-state NMR study and assignments of the KcsA potassium ion channel of S. lividans. *Biochimica et Biophysica Acta (BBA) - Proteins and Proteomics.* **1774** (12), 1604-1613 (2007).

39. Zhang, D., Howarth, G. S., Parkin, L. A., McDermott, A. E. NMR studies of lipid regulation of the K+ channel KcsA. *Biochimica et Biophysica Acta (BBA) - Biomembranes.* 183491 (2020).

40. Schneider, R. et al. Solid-state NMR spectroscopy applied to a chimeric potassium channel in lipid bilayers. *Journal of the American Chemical Society.* **130** (23), 7427-7435 (2008).

41. Raleigh, D. P., Levitt, M. H., Griffin, R. G. Rotational resonance in solid-state Nmr. *Chemical Physics Letters.* **146** (1-2), 71-76 (1988).

42. Schaefer, J., Stejskal, E. O. C-13 nuclear magnetic-resonance of polymers spinning at magic angle. *Journal of the American Chemical Society.* **98** (4), 1031-1032 (1976).

43. Fung, B. M., Khitrin, A. K., Ermolaev, K. An improved broadband decoupling sequence for liquid crystals and solids. *Journal of Magnetic Resonance.* **142** (1), 97-101 (2000).

44. Weingarth, M., Bodenhausen, G., Tekely, P. Low-power decoupling at high spinning frequencies in high static fields. *Journal of Magnetic Resonance.* **199** (2), 238-241 (2009).

45. Loquet, A., Tolchard, J., Berbon, M., Martinez, D., Habenstein, B. Atomic scale structural studies of macromolecular assemblies by solid-state nuclear magnetic resonance spectroscopy. *Journal of Visualized Experiments: JoVE.* (127) (2017).

46. Zhou, D. H., Rienstra, C. M. High-performance solvent suppression for proton detected solid-state NMR. *Journal of Magnetic Resonance.* **192** (1), 167-172 (2008).

47. Baldus, M., Petkova, A. T., Herzfeld, J., Griffin, R. G. Cross polarization in the tilted frame: assignment and spectral simplification in heteronuclear spin systems. *Molecular Physics.* **95** (6), 1197-1207 (1998).

48. Verel, R., Baldus, M., Ernst, M., Meier, B. H. A homonuclear spin-pair filter for solid-state NMR based on adiabatic-passage techniques. *Chemical Physics Letters.* **287** (3-4), 421-428 (1998).

49. Lewandowski, J. R., Sass, H. J., Grzesiek, S., Blackledge, M., Emsley, L. Site-specific measurement of slow motions in proteins. *Journal of the American Chemical Society.* **133** (42), 16762-16765 (2011).

50. Sauvee, C. et al. Highly efficient, water-soluble polarizing agents for dynamic nuclear polarization at high

frequency. *Angewandte Chemie (International Edition in English).* **52** (41), 10858-10861 (2013).

51. Zhai, W. et al. Postmodification via thiol-click chemistry yields hydrophilic trityl-nitroxide biradicals for biomolecular high-field dynamic nuclear polarization. *The Journal of Physical Chemistry. B.* **124** (41), 9047-9060 (2020).
52. Ghosh, R., Kragelj, J., Xiao, Y., Frederick, K. K. Cryogenic sample loading into a magic angle spinning nuclear magnetic resonance spectrometer that preserves cellular viability. *Journal of Visualized Experiments: JoVE.* (163) (2020).
53. Narasimhan, S. et al. Characterizing proteins in a native bacterial environment using solid-state NMR spectroscopy. *Nature Protocols.* In Press (2020).
54. Ni, Q. Z. et al. High frequency dynamic nuclear polarization. *Accounts of Chemical Research.* **46** (9), 1933-1941 (2013).
55. Weingarth, M. et al. Quantitative analysis of the water occupancy around the selectivity filter of a K+ channel in different gating modes. *Journal of the American Chemical Society.* **136** (5), 2000-2007 (2014).
56. Lalli, D. et al. Proton-based structural analysis of a heptahelical transmembrane protein in lipid bilayers. *Journal of the American Chemical Society.* **139** (37), 13006-13012 (2017).
57. Schubeis, T. et al. A beta-barrel for oil transport through lipid membranes: Dynamic NMR structures of AlkL. *Proceedings of the National Academy of Sciences of the United States of America.* **117** (35), 21014-21021 (2020).
58. Baker, L. A., Daniels, M., van der Cruijsen, E. A. W., Folkers, G. E., Baldus, M. Efficient cellular solid-state NMR of membrane proteins by targeted protein labeling. *Journal of Biomolecular NMR.* **62** (2), 199-208 (2015).
59. Linser, R. et al. Proton-detected solid-state NMR spectroscopy of fibrillar and membrane proteins. *Angewandte Chemie (International Edition in English).* **50** (19), 4508-4512 (2011).
60. Shukla, R. et al. Mode of action of teixobactins in cellular membranes. *Nature Communications.* **11** (1), 2848 (2020).
61. Kaplan, M. et al. Probing a cell-embedded megadalton protein complex by DNP-supported solid-state NMR. *Nature Methods.* **12** (7), 649-652 (2015).
62. Visscher, K. M. et al. Supramolecular organization and functional implications of K(+) channel clusters in membranes. *Angewandte Chemie (International Edition in English).* **56** (43), 13222-13227 (2017).
63. Narasimhan, S. et al. DNP-supported solid-state NMR spectroscopy of proteins inside mammalian cells. *Angewandte Chemie (International Edition in English).* **58** (37), 12969-12973 (2019).
64. Wu, R., Stephenson, R., Gichaba, A., Noinaj, N. The big BAM theory: An open and closed case? *Biochimica et Biophysica Acta (BBA) - Biomembranes.* **1862** (1), 183062 (2020).